Journal of Power Sources, 37 (1992) 369–377

The lithium polymer electrolyte battery VI. Design and characterization of prototypes

F. Capuano, F. Croce and B. Scrosati
Dipartimento di Chimica, Università di Roma 'La Sapienza', Rome (Italy)

(Received June 12, 1991; in revised from July 26, 1991)

Abstract

Flat, thin-film prototypes of rechargeable lithium batteries have been realized using a PEO-based composite polymer electrolyte and composite cathodic mixtures. The performance and the characteristics of these batteries have been investigated by electrochemical and impedance analysis.

Introduction

High-temperature (i.e. around 120 °C) flat-type lithium batteries using poly(ethylene oxide) PEO-based polymer electrolytes and composite cathodes incorporating an intercalation compound, are of potential interest for electric vehicle traction. In previous papers [1–3] we have shown that the use of polymer electrolytes, modified by the addition of finely dispersed, low grain size ceramic powders in conjunction with composite, plastic-like cathodic films, may lead to the realization of improved thin-film, rechargeable lithium batteries.

In this work laboratory prototypes have been realized in flat thin-layer configurations and tested by electrochemical and impedance analyses. The results confirm that thin-layer, lithium polymer batteries do indeed show promising performance in terms of energy content and cyclability.

Experimental

Composite cathodes, containing V_6O_{13} (kindly provided by Harwell Laboratories, UK) or amorphous LiV_3O_8, (prepared according to ref. 4), acetylene black, PEO (BDH, MW 4×10^6) and $LiClO_4$ (Fluka reagent grade product) were prepared by casting the appropriate acetonitrile slurry onto a nickel (high purity Leico Industries Inc. foil with a thickness of 50 μm) current collector. The resulting composite cathodes had the composition of 50 wt.% of cathodic material, 10 wt.% of acetylene black and 40 wt.% of PEO–$LiClO_4$, with a total capacity load of about 10 mA h cm^{-2} (based on a value of 360 mA h g^{-1} for V_6O_{13}) and of about 4 mA h cm^{-2} (based on a value of 270 mA h g^{-1} for LiV_3O_8).

Sheets of the electrolytes, either pure PEO–$LiClO_4$ ([EO units]/[Li] = 8) or composite PEO–$LiClO_4$ ([EO units]/[Li] = 8) + 10% $\gamma LiAlO_2$ were cast from acetonitrile solution onto teflon containers, following a previously described procedure [1].

0378-7753/92/$5.00

Battery prototypes using a lithium foil anode (Foote Mineral Company) with an active area of about 25 cm^2 were constructed and sealed under vacuum in a dry box (humidity content less than 10 ppm) using a combination of heat and pressure. The procedure for assembling the battery prototypes was based on the following sequential steps:

(i) the composite cathode mixture was laminated onto a nickel current collector (positive terminal);

(ii) the electrolyte film was placed on top of the cathodic mixture and then the whole combination was heated to 100 °C; at this temperature the electrolyte film became soft and collapsed on the cathode, thus assuring good adherence and contact;

(iii) the lithium foil was placed on top of the electrolyte film and the cell was completed by a second nickel current collector (negative terminal);

(iv) the cell was compacted by light mechanical pressure and housed in an aluminum 'coffee bag' envelope. The envelope was sealed under vacuum and the prototype removed from the dry box for the electrochemical test.

The schematic diagram of the structure of the polymeric battery prototype is shown in Fig. 1 and its final form in Fig. 2. The packaged cells were placed in an oven at 100 °C for assuring thermal control during the electrochemical characterization.

The impedance measurements were carried out with a Solartron 1255 frequency response analyser in combination with a Solartron 1286 electrochemical interface, over a frequency of range 100 kHz to 1.0 mHz. The entire equipment was dynamically controlled by a personal computer used both for the opitimization of the measurement and for data collection. A fitting analysis of the experimental impedance data was performed using the Boukamp's [5] program equivalent circuit. All the impedance measurements on cycled cells both in the discharged or charged state, were carried out following a 30 min equilibration under open circuit voltage (OCV), in order to eliminate polarization effects.

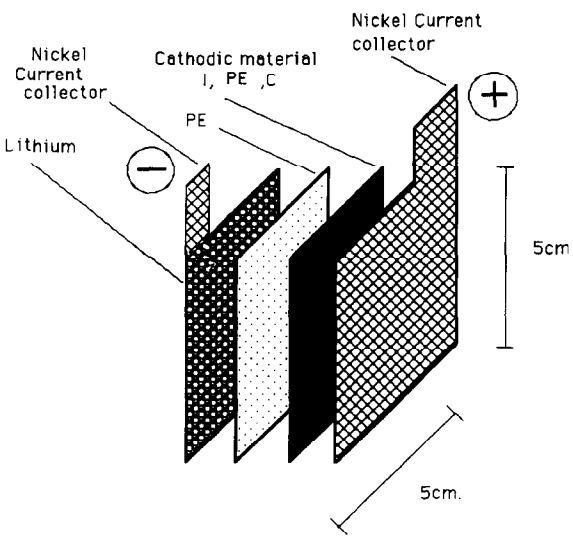

Fig. 1. Schematic diagram of the structure of prototypes of polymer, flat-type, thin-film, lithium batteries.

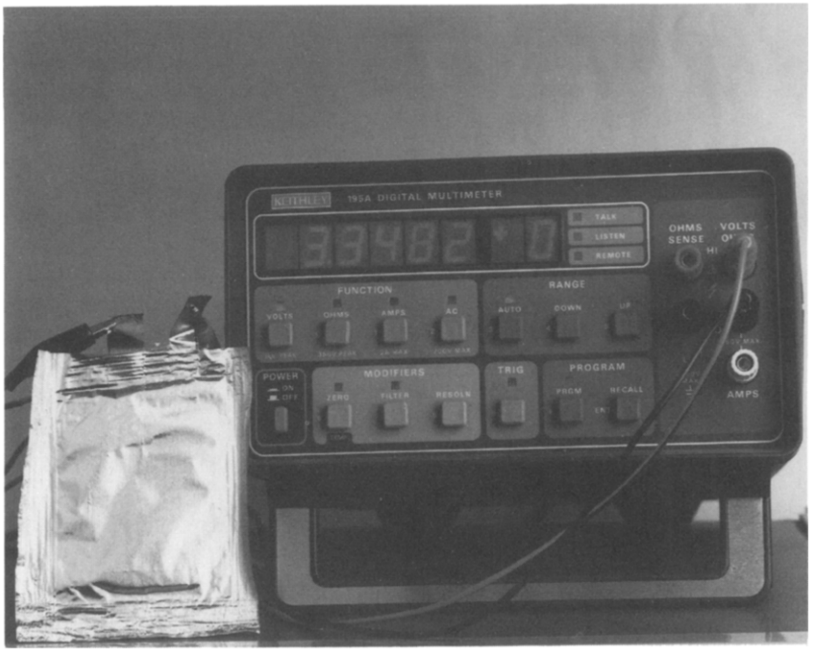

Fig. 2. Packaged polymeric lithium battery prototype.

The current voltage polarization curves were obtained using a Solartron 1286 electrochemical interface. The cycling tests were performed by an automatic voltage-controlled inverter (Amel model 545) at constant current between preset voltage limits. All data were collected and stored with a HP Vectra personal computer.

Results and discussion

We have assembled flat-type, lithium battery prototypes of the following general composition:

$Li/(PEO)_8LiClO_4\gamma LiAlO_2/(PEO)_8LiClO_4,C,I$

where

- Li is a lithium foil anode (about 1 mm thick)
- $(PEO)_8LiClO_4\gamma LiAlO_2$ is a film (about 100 μm thick) of a composite polymer electrolyte, formed by adding to the 'classical' PEO–$LiClO_4$ complex [6], 10 weight percent (wt.%) of finely dispersed $\gamma LiAlO_2$ ceramic powder [3];
- $(PEO)_8LiClO_4$,C,I, is a film (about 250 μm thick) of a composite cathode formed by casting from an acetonitrile slurry a mixture of $(PEO)_8LiClO_4$ electrolyte, carbon and the active intercalation compound I [2]. For the latter we have used the vanadium bronze LiV_3O_8 or, alternatively, the vanadium oxide V_6O_{13}.

Figure 3 shows the impedance response at 100 °C of a prototype battery using the vanadium oxide-based (curve a) and the vanadium bronze based (curve b) cathode mixture. The intercept with the real axis identifies the resistance of the electrolyte R_i, which as a first approximation may be considered as the internal resistance of the

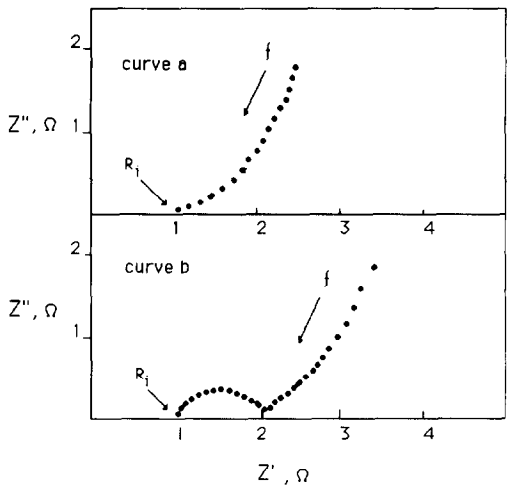

Fig. 3. Impedance response of the Li/V_6O_{13} (curve a) and Li/LiV_3O_8 (curve b) battery prototypes at 100 °C. The intercept R_i with the real axis Z' may be considered as the prototype internal resistance.

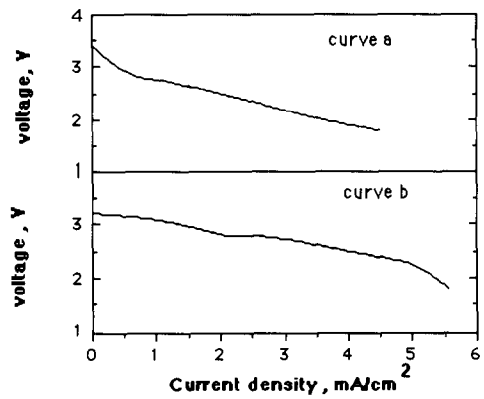

Fig. 4. Voltage–current polarization curve of the Li/V_6O_{13} (curve a) and Li/LiV_3O_{13} (curve b) battery prototypes at 100 °C.

prototype. The obtained values are low (around 4×10^{-2} Ω cm^{-2}), i.e. comparable with those reported by other laboratories involved in the development of high-performance, lithium polymer batteries [7, 8]. The low impedance of the prototypes confirms that the polymer electrolyte used has a high ionic conductivity and that the composite cathodes have adequate electronic conductivity [9].

Figure 4 illustrates the polarization curves of battery prototypes using the two vanadium intercalating compounds. The curves were obtained by discharging the prototype at progressively higher current densities and recording the acquired voltage values. We notice that in both cases the prototypes may sustain discharge rates up to 6 mA cm^{-2} before undergoing concentration polarization. In addition, the slopes of the initial part of Figure 4 indicate that the internal resistance of the batteries has

a low value, confirming the results already discussed with the impedance analysis (Fig. 3).

Figure 5 illustrates the first discharge curve of a Li/LiV_3O_8 prototype at 0.4 mA cm^{-2} (i.e. at a $C/10$ rate) and between preset voltage limits of 1.8–3.4 V. Under these conditions, the battery delivered a capacity which, within the experimental error, approached the theoretical value. This result is further confirms that the thin-layer polymer battery prototypes are characterized by good electrochemical performance, as previously evidenced in smaller-scale laboratory cells [10].

However, this performance tends to somewhat decay upon prolonged operation. Figure 6 shows the response of the Li/LiV_3O_8 prototype under various cycling conditions. One may clearly notice that a high fraction of the theoretical capacity is delivered only during the few initial cycles, after which a consistent decline in capacity takes place. This effect, which is typical of Li polymeric batteries [11], is not related to a degradation of the polymer electrolyte transport properties, but rather to a deterioration of the electrodic interfaces.

This important conclusion is supported by various experimental results, namely the modification of the trend of the charge and discharge curves observed during the

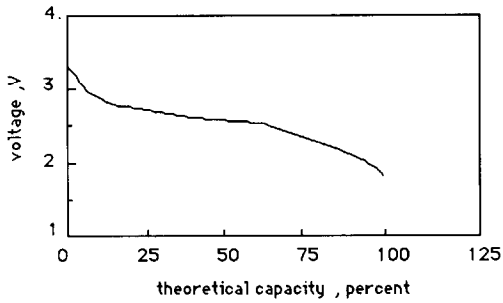

Fig. 5. First discharge of a Li/LiV_3O_8 battery prototype. Current density 0.4 mA/cm^{-2}. Temperature 90 °C.

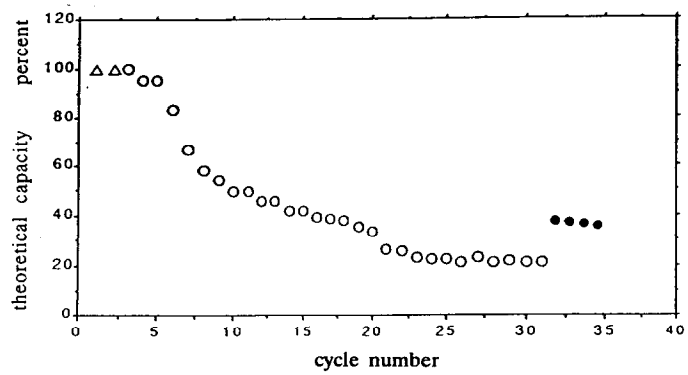

Fig. 6. Capacity behaviour of Li/LiV_3O_8 battery prototype upon cycling at different conditions. △: Charge current density 0.2 mA cm^{-2}; discharge current density 0.2 mA cm^{-2}; T=90 °C. ○: Charge current density 0.2 mA cm^{-2}; discharge current density 0.2 mA cm^{-2}; T=120 °C. ●: Charge current density 0.1 mA cm^{-2}; discharge current density 0.1 mA cm^{-2}; T=120 °C.

progressive cycling test, as well as by impedance analysis of the battery taken at various stages of its cycling life.

Figure 7(a) shows the trend of the 9th cycle: well defined charge–discharge profiles, with good coulombic efficiency are still obtained, even if a certain decline in delivered capacity has already occurred (see Fig. 6). Figure 7(b) illustrates the discharge–charge profile of the 16th cycle. The erratic trend of the final charging voltage plateau is here evident and even more dramatic in the following cycles, as demonstrated by Fig. 7(c), which illustrates the profile of the 18th cycle.

This effect may be associated to the growth of lithium microdendrites across the cell, in turn related to passivation phenomena occurring at the negative interface: part of the charging current may be dissipated through these dendrites with an associated fraction of charge which is no longer available for the expected charging process, namely the de-intercalation of lithium form the vanadium bronze. Consequently, in the following discharge cycle the battery delivers only a part of the total 'apparent' received charge since only that fraction of the total charge which effectively goes to recharge the cell may be delivered back. Therefore, the 'apparent' capacity recovery remains necessarily lower than the expected theoretical one. The process is cumulative and the practical result is a progressive decline in capacity, as was observed experimentally (Fig. 6).

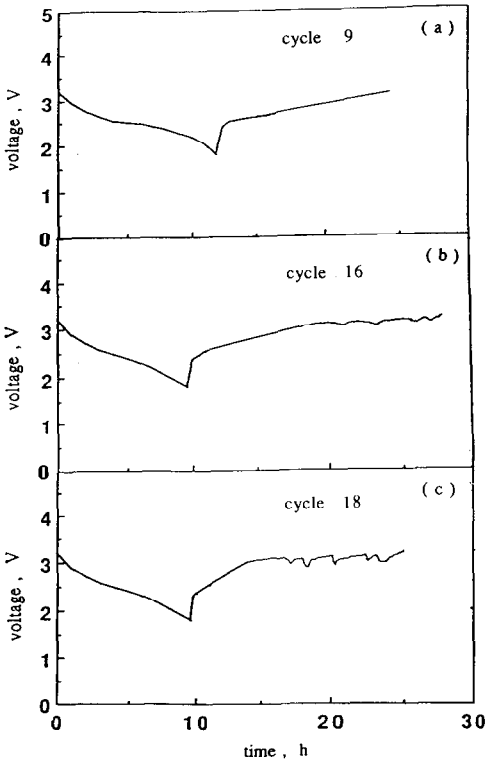

Fig. 7. Charge–discharge profile of the 9th (curve a), 16th (curve b), and 18th (curve c) cycle of a Li/LiV_3O_8 battery prototype. Current density: 0.2 mA cm^{-2}. Temperature 120 °C. Voltage limits 1.8–3.2 V.

This interpretation is somewhat confirmed by the analysis of the trend of the charge–discharge coulombic efficiency ratio obtained upon cycling and illustrated in Fig. 8. One clearly notices that in the cycling range where the decline in capacity is particularly severe (e.g. around cycles 15 to 23, see Fig. 6) an efficiency ratio much higher than one (a dashed horizontal line corresponding to charge/discharge efficiency equal to 1 is drawn as a reference for the eye) is formally obtained, thus supporting the idea that part of the charge consumed in the charging process is only apparently directed to the restoration of the electrochemical process, while effectively being deviated along the dendrite shunts.

Further support for this model is provided by impedance analysis. Figure 9 compares the impedance response of a Li/LiV_3O_8 battery prototype after the 1st (curve a) and the 18th (curve b) cycles. A substantial modification upon cycling of the response is clearly evident: the semicircle which is representative of the interfacial characteristics progressively expands to then split into two relaxation arcs, both effects being generally accepted as convincing evidence of an increase of the interfacial resistance due to the growth of a passivation layer on the electrode surface [11, 12].

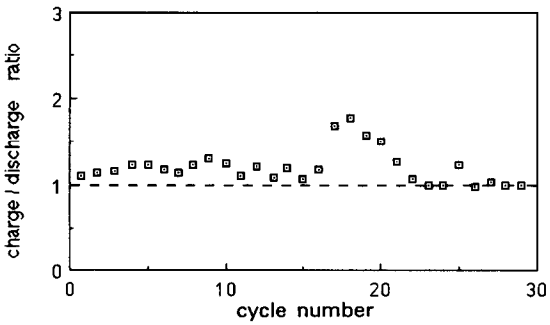

Fig. 8. Apparent charge–discharge efficiency ratio during cycling of the Li/LiV_3O_8 battery prototype.

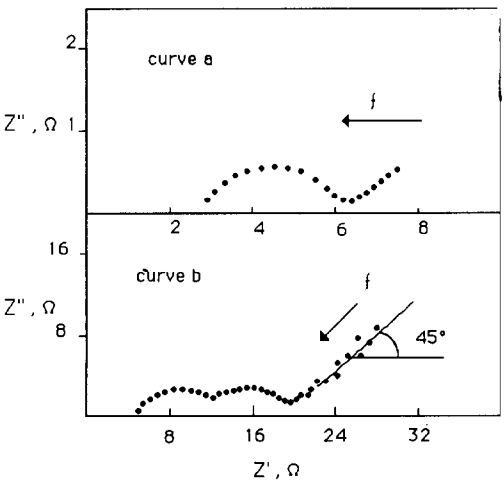

Fig. 9. Impedance response at 90 °C of the Li/LiV_3O_8 prototype after the 1st (curve a) and the 18th (curve b) cycle.

From the impedance plots of Fig. 9 one may also identify a 45 degree line at low frequencies, which is generally representative of mass-transport kinetics [13] and thus, in the present case, representative of the Li^+ ion diffusion across the electrolyte and throughout the intercalation LiV_3O_8 electrode. Therefore, loss of capacity, also due to slow diffusion kinetics of the electrochemical process of Li^+ intercalation into the intercalation electrode particles, cannot be excluded. Confirmation of this possibility lies in the fact that, if the cycling rates are decreased thus allowing the evolution of slow processes, an extra fraction of the theoretical capacity can be recovered, as shown by the last cycles reported in Fig. 6. The charging rate for these cycles was decreased by a factor of one half with respect to the preceding ones and indeed the fraction of theoretical capacity obtained in discharge rose from 20% to 40%.

Finally, a third effect causing the capacity decline upon cycling could be the electrical isolation of some of the electrode particles throughout the composite positive membrane, resulting from the repeated intercalation–deintercalation cycles and related changes in volume of the electrodic mass.

Conclusions

Lithium polymer battery prototypes are in principle capable of excellent performance, in terms of high-power output (see Fig. 4), high discharge utilization (see Fig. 5) and high charge–discharge efficiency (see initial cycles of Fig. 6).

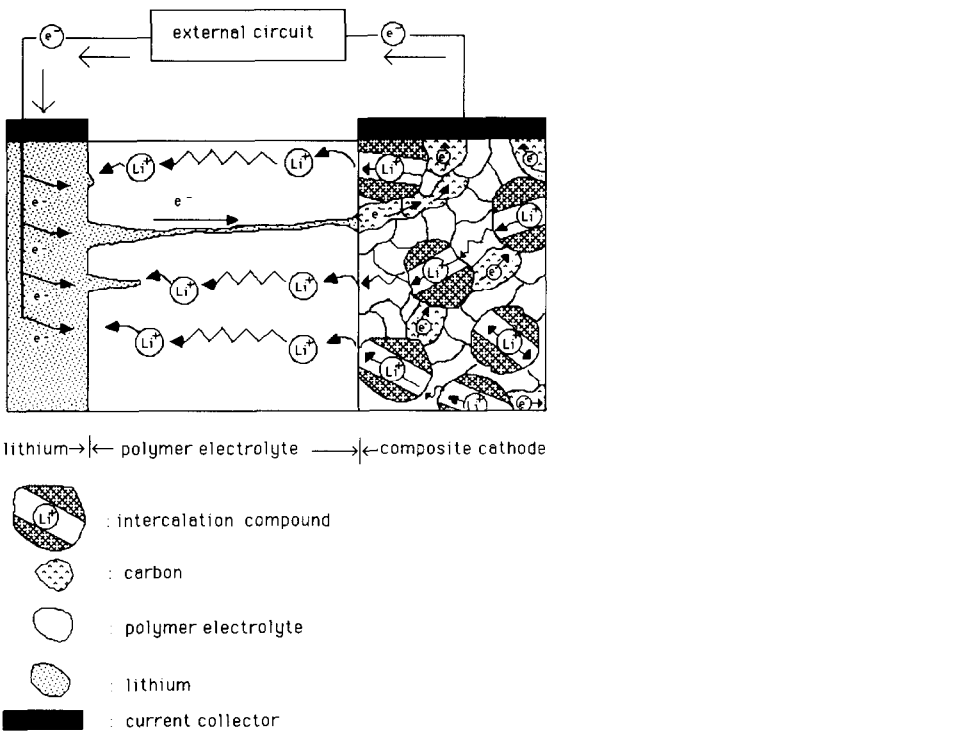

Fig. 10. Pictorical illustration of the model of the charging process in polymer electrolyte batteries. Part of the capacity is lost by shunt along dendrites and by electrical isolation of some intercalation compound particles.

However, upon prolonged operation, the batteries suffer a progressive decline in delivered capacity. This may be a serious drawback, certainly worthy of careful consideration and precise clarification. We propose here a model to account for this capacity decline, which is pictorially summarized and illustrated in Fig. 10. According to this model, the loss in capacity may be in part apparent—i.e. due to the fact that a fraction of the charging current is shunted along lithium microdendrites and thus not available for driving the electrochemical process—and in part real—i.e. associated with an electrical isolation of particles of the intercalation active compound in the positive electrode composite mixture.

On the basis of this model, we suggest some strategies for modification of the basic structure of the polymer battery with the final goal of improving its performance. These strategies are, in essence:

(i) Modification of the electrolyte and electrode configuration and nature, in order to reduce the passivation phenomena. These modifications could be accomplished with a careful purification of the components in order to minimize the amount of residual impurities, such as water of high-vapour pressure solvents, which are well-known corrosive agents towards lithium.

(ii) Optimization of the composite cathode morphology and composition to improve homogeneity among the components. This optimization could be accomplished by a reduction of the particle size of the intercalation compounds, by the determination of its most suitable concentration and the realization of improved mixing techniques.

The two main strategies are under evaluation in our laboratory and the results will be discussed and evaluated in future papers.

Acknowledgement

This work was carried out with the financial support of the Comitato Nazionale per la Ricerca e lo Sviluppo della Energia Nucleare e delle Energie Alternative (ENEA), contratto ENEA-Dipartimento di Chimica.

References

1 F. Croce, F. Capuano, A. Selvaggi and B. Scrosati, *J. Power Sources, 32* (1990) 381.
2 A. Selvaggi, F. Croce and B. Scrosati, J. Power Sources, 32 (1990) 389.
3 F. Capuano, F. Croce and B. Scrosati, *J. Electrochem. Soc., 138* (1991) 1918.
4 G. Pistoia, M. Pasquali, Y. Geranov, V. Manev and R. V. Moshtev, *J. Power Sources, 27* (1989) 35.
5 B. A. Boukamp, *Solid State Ionics, 11* (1984) 339.
6 J. R. MacCallum and C. A. Vincent (eds.), *Polymer Electrolyte Reviews,* Vols. I and II, Elsevier Applied Science, London, 1987 and 1989.
7 R. J. Neat, W. J. Macklin and R. J. Powell, in B. Scrosati (ed.), *Proc. 2nd Int. Symp. Polymer Electrolytes,* Elsevier Applied Science, London, 1990, p. 421.
8 J. S. Lundsgaard, S. Yde-Andersen, R. Koksband, D. R. Shackle, R. A. Austin and D. Fauteux, *Proc. 2nd Int. Symp. Polymer Electrolytes,* Elsevier Applied Science, London, 1990, p. 306.
9 W. J. Macklin, R. J. Neat and R. J. Powell, *J. Power Sources, 34* (1991) 39.
10 F. Bonino, M. Ottaviani, B. Scrosati and G. Pistoia, *J. Electrochem. Soc., 135* (1988) 12.
11 B. Scrosati, *J. Electrochem. Soc., 136* (1989) 2774.
12 D. Fauteux, *J. Electrochem. Soc., 135* (1988) 2231.
13 J. Ross Macdonald (ed.), *Impedance Spectroscopy,* Wiley, New York, 1987.